COMMUNICATIONS IN NUMERICAL METHODS IN ENGINEERING
*Commun. Numer. Meth. Engng* (2009)
Published online in Wiley InterScience (www.interscience.wiley.com). DOI: 10.1002/cnm.1259

# A quadratic least-squares solution reconstruction in a boundary layer region

N. B. Petrovskaya*, †

*School of Mathematics, University of Birmingham, Edgbaston, Birmingham B15 2TT, U.K.*

SUMMARY

A local weighted least-squares (LS) method is often used to approximate a solution function in computational aerodynamics problems. In our paper we study LS approximation by a quadratic polynomial on unstructured grids that have the high cell aspect ratio. It will be shown in the paper that an LS method degrades to unacceptable accuracy on stretched meshes and weighting of distant stencil points does not result in a more accurate reconstruction. A concept of numerically distant points will be employed to explain the reasons behind the method's poor performance and an approach will be discussed that allows one to improve the results of a quadratic LS reconstruction in a boundary layer region. Copyright © 2009 John Wiley & Sons, Ltd.

Received 15 July 2008; Revised 7 March 2009; Accepted 10 March 2009

KEY WORDS: weighted least-squares approximation; quadratic reconstruction; stretched mesh; anisotropic solution function

## 1. INTRODUCTION

In past decades, a method of local least-squares (LS) approximation has received a lot of attention in computational aerodynamics [1–6]. The need in local LS approximation is based on a growing demand to employ higher-order discretization schemes for numerical solution of complex aerodynamics problems [1, 2, 7–9]. Higher-order finite volume schemes are a class of discretization schemes where an LS method is frequently employed, as they require a local reconstruction of the solution gradient [2, 10, 11], and an LS method allows one to reconstruct a function at a given point of a computational grid by using data that are readily available at neighboring grid

*Correspondence to: N. B. Petrovskaya, School of Mathematics, University of Birmingham, Edgbaston, Birmingham B15 2TT, U.K.
†E-mail: n.b.petrovskaya@bham.ac.uk

Contract/grant sponsor: The Boeing Company; contract/grant number: 66-ZB-B001-10A-533

points. Usually a function reconstruction is made by a polynomial of a chosen degree where the polynomial coefficients are determined from the solution of a local LS problem.

The accuracy of a local LS reconstruction is considered as a priority requirement, as a reconstructed function should be further used for iterative solution of the governing equations of a computational aerodynamic problem. An LS method on regular grids is usually regarded as the accurate means of function approximation (e.g. see [12, 13]). Meanwhile, in many practical applications it is required to reconstruct a function on highly anisotropic unstructured meshes that are generated about an airfoil. In the latter case the implementation of an LS reconstruction in the problem may encounter serious difficulties. It has recently been demonstrated in [4, 6, 14] that an LS method degrades to unacceptable accuracy on stretched meshes. Furthermore, it has been discussed in [4, 14] that the poor accuracy of an LS reconstruction affects the convergence of an approximate solution by generating large discretization errors and ill-conditioned matrices. Thus, the conclusions about the accuracy of an LS reconstruction should be revised if irregular meshes are employed.

A detailed discussion of an LS method on highly anisotropic grids has been provided in recent paper [6] for an LS reconstruction by a linear polynomial. In the present paper, we continue the study of an LS method for the case when LS approximation by a quadratic polynomial is exploited in the problem. To our best knowledge, a problem of a higher-order LS reconstruction on anisotropic meshes has not been discussed in the literature yet, as a main research effort on a local LS reconstruction has been concentrated on structured meshes and regular unstructured meshes so far (e.g. see [3, 5, 15]). Meanwhile, our numerical experience with a quadratic LS reconstruction used in practical computations is that the method generates a very inaccurate solution when a solution function is reconstructed on a stretched mesh near an airfoil. Hence, using a higher-order polynomial in an LS problem does not result in a more accurate reconstruction on irregular grids, and further careful study of an LS method on anisotropic unstructured meshes is required.

A large reconstruction error is often attributed to the presence of geometrically distant points that appear in a reconstruction stencil on grids with the high cell aspect ratio. Thus, a frequent recommendation is to assign weights to stencil points, where a weight function is defined as a function of the Euclidian distance between two points in order to mitigate the impact of distant points on the accuracy of LS approximation [2, 3, 5, 16]. However, despite the success of this approach for many test case problems, it turned out that weighting of stencil points is not efficient on anisotropic meshes used in practical computations. It has been discussed in [6, 14] that the results of a weighted linear LS reconstruction can be worse than those for an unweighted reconstruction. In our paper, we expand the above conclusion to a quadratic reconstruction by making direct comparison of the results of a weighted and unweighted reconstruction on irregular meshes.

In work [6], a concept of numerically distant points has been introduced to explain the poor accuracy of a weighted LS method on stretched meshes. A numerically distant point is a point that can be located close to the origin where a reconstruction is made, but it still has a large error in data required for the reconstruction. It has been demonstrated in [6] that in regions where the solution has a strong gradient (e.g. in a boundary layer) numerically distant points often appear in a reconstruction stencil. Those regions usually require generation of an anisotropic mesh to resolve the solution gradient, so that the poor performance of the method is associated with a stretched mesh geometry. While geometrically distant points can be easily suppressed by means of simple geometric weighting, it is still unclear how to get rid of numerically distant points in a reconstruction stencil. It has been suggested in [6] that one approach to eliminate them from a linear LS reconstruction is to use a compact stencil where the number of stencil points will be minimized.



DOI: 10.1002/cnm

A quadratic reconstruction, however, represents a more difficult case, as a compact stencil does not generally provide a number of degrees of freedom required for a quadratic polynomial. Thus, in our paper we discuss an approach to a quadratic reconstruction on a compact stencil where additional information about a solution function can be used to compute all degrees of freedom. This idea is illustrated by consideration of an 'anisotropic' function where the knowledge of a gradient direction allows one to determine the polynomial coefficients for a quadratic reconstruction.

## 2. A LOCAL LS SOLUTION RECONSTRUCTION

Consider a two-dimensional domain $\Omega$ where an unstructured computational grid $G$ is generated about an airfoil (see Figure 1(a)). Let points $P_n = (x_n, y_n) \in G,\ n = 1, \ldots, N_G$, and data vector $\mathbf{U}_G$ be defined at points $P_n$, where $U_n = U(P_n)$. The vector $\mathbf{U}_G$ is usually thought of as a solution to governing equations of a computational aerodynamics problem that is numerically solved on grid $G$.

We now define another set of points $\{\bar{P}_l\}$, $l = 1, \ldots, L$, over the grid $G$, where the data $\mathbf{U}_G$ will be approximated at each point $\bar{P}_l$ by an LS method. The definition of the set $\{\bar{P}_l\}$ is based on a given problem under consideration. Below we discuss a computational problem where the solution $\mathbf{U}_G$ is defined at nodes of grid $G$, and the set $\{\bar{P}_l\}$ consists of all edge midpoints taken on $G$. Such a definition of the points $\{\bar{P}_l\}$ is often related to node-centered discretization schemes.

Let $\bar{P}_l$ be the edge midpoint at edge $e_l$. For a local LS reconstruction at point $\bar{P}_l$, a reconstruction stencil $S_l$ is allocated as follows. The two nodes $n_1$ and $n_2$ that comprise the edge $e_l$ are identified, and the stencil $S_l$ composes all grid nodes that belong to edges incident to the node $n_1$ or $n_2$ (stencil $I$ in Figure 2). Generally, the number $N$ of stencil points is different for two different points $\bar{P}_{l_1}$ and $\bar{P}_{l_2}$, as it depends on the geometry of a computational grid. Some computational problems may also require an expanded reconstruction stencil, in which case 'neighbors of neighbors' are

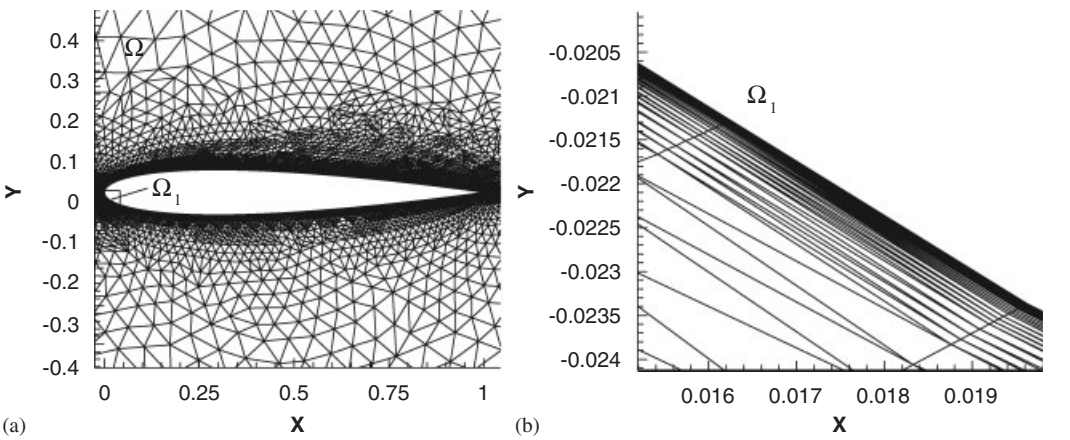


Figure 1. (a) An unstructured grid generated about an airfoil. (b) A grid fragment near the wall (the domain $\Omega_1$ in (a)). A grid with the high cell aspect ratio should be generated to resolve the solution in the direction normal to the wall.



DOI: 10.1002/cnm

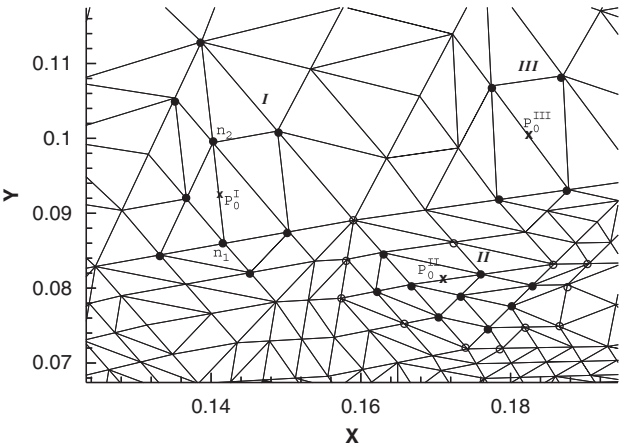


Figure 2. Examples of a reconstruction stencil for local LS approximation at a given edge midpoint. Stencil members are shown as black circles. A stencil (I) used for the reconstruction at point $P_0^{\mathrm{I}}$ composes all grid nodes that belong to edges incident to the node $n_1$ or $n_2$. An expanded stencil (II) generated for $P_0^{\mathrm{II}}$ also includes 'neighbors of neighbors' shown as empty circles in the figure. A compact stencil (III) consists of four grid nodes belonging to the adjacent cells that share a given edge.

considered to select the next layer of grid nodes for stencil $S_l$. One example of an expanded reconstruction stencil is shown in Figure 2 (see stencil II in the figure).

Once a reconstruction stencil $S_l$ has been defined, the point $\bar{P}_l$ is denoted as $P_0$ and the stencil points are locally numbered as $P_1$ through $P_N$. Consequently, a local data vector $\mathbf{U}=(U_1, U_2, \ldots, U_N)$ is allocated by taking the entries of $\mathbf{U}_G$ at stencil points. A local LS solution reconstruction is then a problem of fitting the data $\mathbf{U}$ to the function

$$u_{\mathrm{LS}}(x, y)=\sum_{k=0}^{M} u_k \phi_k(x, y), \quad M<N \tag{1}$$

where $\mathbf{u}=(u_0, u_1, u_2, \ldots, u_M)$ are fitting parameters and $\phi_k(x, y)$, $k=0, \ldots, M$, are polynomial basis functions. In our paper we consider the approximation by a quadratic polynomial,

$$u_{\mathrm{LS}}(x, y)=u_0+u_1(x-x_0)+u_2(y-y_0)+u_3(x-x_0)^2+u_4(x-x_0)(y-y_0)+u_5(y-y_0)^2 \tag{2}$$

where we have $u_{\mathrm{LS}}(P_0)=u_0$.

The unknown parameters $\{u_k\}$ are determined in the LS method by seeking the minimum of the merit function,

$$F^2=\min_{\mathbf{u}} \sum_{i=1}^{N} [U(P_i)-u(P_i)]^2$$

Taking the partial derivatives of the function $F^2$ with respect to the fitting parameters $u_k$ results in $M+1$ normal equations

$$\sum_{i=1}^{N} \left[ U_i - \sum_{j=0}^{M} u_j \phi_j(P_i) \right] \phi_k(P_i)=0, \quad k=0, \ldots, M$$



DOI: 10.1002/cnm

Introducing the design matrix $\mathbf{A}$ as $A_{ij}=\phi_j(P_i), \quad i=1,\ldots,N,\ j=0,\ldots,M$, the normal equations are solved for the vector $\mathbf{u}$

$$\mathbf{u}=\mathbf{A}_{\mathrm{LS}}^{-1}\mathbf{b}_{\mathrm{LS}} \tag{3}$$

where the matrix $\mathbf{A}_{\mathrm{LS}}=\mathbf{A}^{\mathrm{T}}\mathbf{A}$ and the vector $\mathbf{b}_{\mathrm{LS}}=\mathbf{A}^{\mathrm{T}}\mathbf{U}$. Once the function $U(x,y)$ has been reconstructed at a given point $P_0\equiv\bar{P}_l$, the next edge midpoint $\bar{P}_{l+1}$ is taken and the reconstruction procedure is repeated until the solution field is reconstructed over the entire grid.

While an LS method reconstructs a smooth function $U(x,y)$ with desired accuracy on a uniform grid [12, 13, 17], the method demonstrates the poor accuracy when the stretched meshes are considered. Below we discuss a numerical example illustrating the difficulties arising when a local LS reconstruction is implemented in a practical computational aerodynamics problem where an anisotropic mesh is generated about an airfoil.

### *2.1. The accuracy of a quadratic reconstruction on irregular meshes*

Consider turbulent flow about an NACA0012 airfoil obtained as a result of numerical solution of the Navier–Stokes equations on a sequence of adaptive unstructured grids generated by an anisotropic grid adaptation procedure [18]. A solution to the system of governing equations is computed by an accurate numerical method (streamline upwind Petrov–Galerkin (SUPG), [19]) that employs higher-order polynomial functions to discretize the equations over a given computational grid $G$. In the test case under consideration, a solution has been obtained for a Mach number of 0.2, a Reynolds number of $9\times10^6$ and an angle of attack of 12.0°. Characteristic boundary conditions have been implemented in a far field, and an isothermal solid wall boundary condition has been considered in a near field. The details of the numerical solution procedure can be found in [9].

In our example, the $x$-component of the velocity vector in the Navier–Stokes equations has been chosen as a scalar solution field $U(x,y)$ to discuss the results of a quadratic LS reconstruction. Let us consider the grid $G_{\mathrm{C}}$ taken from the sequence of grids used in the solution grid adaptation algorithm. This 'coarse' grid shown in Figure 1(a) is a very irregular grid as would generally be the case for an unstructured adaptive grid code. The maximum cell aspect ratio on grid $G_{\mathrm{C}}$ is $10^3$, with the distance of the first point normal to the wall being $8\times10^{-6}$ chords. For the purpose of our study we then generate a new grid $G$ by uniform refinement of the grid $G_{\mathrm{C}}$, so that all edge midpoints on coarse grid $G_{\mathrm{C}}$ become grid nodes on fine grid $G$ (see Figure 3, where an example of uniform refinement is given). The coarse grid $G_{\mathrm{C}}$ has $N_{G_{\mathrm{C}}}=6270$ grid nodes, while the grid $G$ used to compute an accurate solution $U(x,y)$ has $N_G=24\,807$ nodes, where $N_G=N_{G_{\mathrm{C}}}+N_{E_{\mathrm{C}}}$, and $N_{E_{\mathrm{C}}}=18\,537$ is the number of edge midpoints on grid $G_{\mathrm{C}}$. The original data structure related to grid $G_{\mathrm{C}}$ is stored, and once the solution has been computed on grid $G$ it is projected onto the coarse grid $G_{\mathrm{C}}$. The function $U(x,y)$ is then reconstructed at edge midpoints of grid $G_{\mathrm{C}}$ by an LS method and the approximation $u_{\mathrm{LS}}(x,y)$ is compared with the solution $U(x,y)$ available at the same grid points on grid $G$ (see Figure 3).

The validation of the accuracy of an LS reconstruction is made based on the following error function $e(x,y)$ computed at points $(x,y)\in\{\bar{P}_l\},\ l=1,\ldots,N_{E_{\mathrm{C}}}$,

$$e(x,y)=|U(x,y)-u_{\mathrm{LS}}(x,y)| \tag{4}$$

where point $P=(x,y)\in G$ and $P\in\{\bar{P}_l\}$. In other words, $P$ is a node on the fine grid $G$ and at the same time $P$ is an edge midpoint on the coarse grid $G_{\mathrm{C}}$. The functions $U(x,y)$ and $u_{\mathrm{LS}}(x,y)$



DOI: 10.1002/cnm

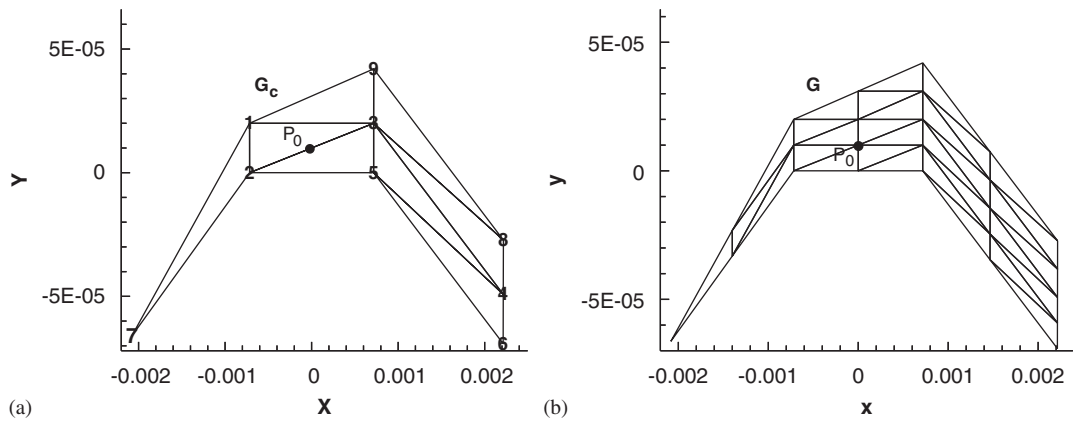


Figure 3. A fragment of a computational grid near the wall. The $y$-axis is scaled for the sake of visualization: (a) a reconstruction stencil for point $P_0$ includes all points $P_1$ through $P_9$ (except point $P_6$) on a coarse grid $G_C$ and (b) the grid $G_C$ is refined and the solution $U(x, y)$ is computed at grid nodes on a fine grid $G$. Once the solution is available at the stencil points, an LS reconstruction is made at point $P_0$ on coarse grid $G_C$ and the value $u_{LS}(P_0)$ is compared with the solution $U(P_0)$ obtained at point $P_0$ on fine grid $G$.

are an accurate SUPG solution and a quadratically reconstructed solution (2), respectively. We are interested in the maximum error (4) in a 'boundary layer' region $D_b$,

$$e_{\max_b} = \max_{(x,y)\in D_b} e(x, y) \tag{5}$$

where $D_b$ is a subgrid of the grid $G$ with nodes $(x, y) : X1 = -0.05 < x < X2 = 1.05$, $Y1 = -0.05 < y < Y2 = 0.05$. Let us notice that despite the actual topology of a boundary layer being different from that of a rectangle $D_b$, we use the name 'boundary layer' to emphasize that a non-uniform grid with the high cell aspect ratio is generated in a computational domain near the airfoil (see the example shown in Figure 1(b)).

The maximum error is also computed in a 'far-field' region $D_f$ as follows:

$$e_{\max_f} = \max_{(x,y)\in D_f} e(x, y) \tag{6}$$

where $D_f$ is a subgrid of the grid $G$ with nodes $(x, y) : R_f = 10.0 < \sqrt{(x-0.5)^2 + y^2} < R_\Omega = 500.0$. Again, the name 'far field' is only used to emphasize that the grid in the domain $D_f$ is quasi-uniform.

A logarithmic error $e^l(x, y)$,

$$e^l(x, y) = \log_{10} \frac{|U(x, y)|}{|u_{LS}(x, y)|} \tag{7}$$

allows one to control the order of the reconstruction error magnitude. The maximum logarithmic error near the wall is defined as

$$e^l_{\max_b} = \max_{(x,y)\in D_b} |e^l(x, y)| \tag{8}$$



DOI: 10.1002/cnm

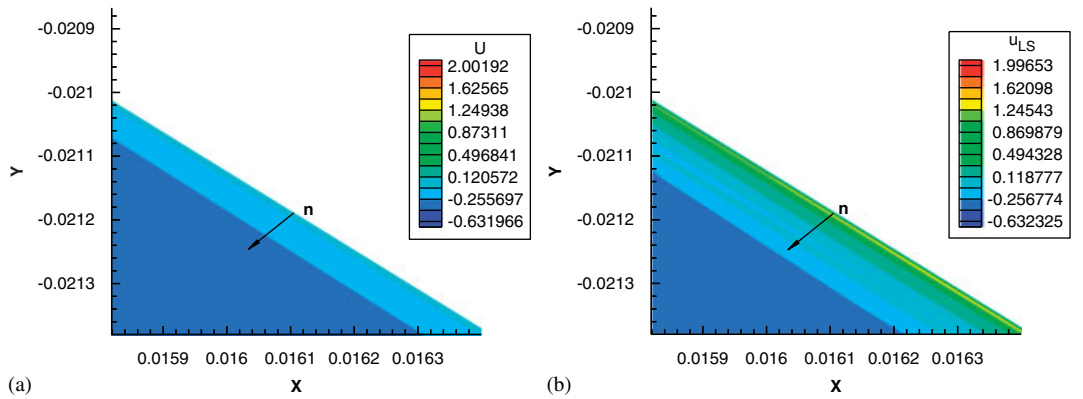


Figure 4. Results of a quadratic LS reconstruction on grid $G$ in grid subdomain near the wall (see also a computational grid shown in Figure 1(b)): (a) an accurate SUPG solution is a monotone function in the direction $\mathbf{n}$ normal to the wall and (b) a quadratic LS reconstruction results in a non-monotone and inaccurate solution on the same grid.

while the maximum logarithmic error in a far field is

$$e^l_{\max_f} = \max_{(x,y)\in D_f} |e^l(x,y)| \tag{9}$$

Our numerical experience with the problem shows that a quadratic LS reconstruction provides accurate results in a far-field region. The maximum error (6) for the reconstruction in domain $D_f$ is $e_{\max_f} \equiv e(x_f, y_f) = 1.2728 \times 10^{-3}$, where $U(x_f, y_f) = 0.9766$, $u_{\mathrm{LS}}(x_f, y_f) = 0.9779$, and the point $P_f = (10.814, 1.269)$. The maximum logarithmic error (9) is $e^l_{\max_f} \equiv |e^l(x_f, y_f)| = 5.6561 \times 10^{-4}$.

Meanwhile, the results of an LS reconstruction near the wall are quite different from those in a far-field region. A grid fragment near the wall has been selected to demonstrate the results of a quadratic reconstruction on an anisotropic grid (see domain $\mathbf{\Omega_1}$ in Figure 1). An accurate SUPG solution is presented in Figure 4(a), while a quadratically reconstructed solution on grid $G$ is shown in Figure 4(b). It can be seen from the figure that an LS reconstruction results in a non-monotone and inaccurate solution near the wall. This conclusion is confirmed by the calculation of a reconstruction error near the wall. The maximum error (5) for a quadratic reconstruction in domain $D_b$ is $e_{\max_b} \equiv e(x_{b_1}, y_{b_1}) = 1.3859$, where $U(x_{b_1}, y_{b_1}) = -3.89462 \times 10^{-2}$, $u_{\mathrm{LS}}(x_{b_1}, y_{b_1}) = 1.34701$, and the point $P_{b_1} = (x_{b_1}, y_{b_1})$ is located close to the wall, $x_{b_1} = 0.0162473$, $y_{b_1} = -0.021828$. The maximum logarithmic error (8) is $e^l_{\max_f} \equiv |e^l(x_{b_2}, y_{b_2})| = 2.49593$, where $x_{b_2} = 0.274632$, $y_{b_2} = -0.059519$ and the solution is $U(x_{b_2}, y_{b_2}) = 2.62319 \times 10^{-1}$, $u_{\mathrm{LS}}(x_{b_2}, y_{b_2}) = 2.9709 \times 10^{-4}$. Hence a quadratic LS reconstruction near the wall degrades to unacceptably poor accuracy on a stretched mesh.

### 2.2. *Weighting of stencil points*

Our next observation about an LS reconstruction in a 'boundary layer' region $D_b$ is that geometric weighting of stencil points does not result in more accurate approximation. This result contradicts a widespread opinion that the poor accuracy of an LS reconstruction should be attributed to geometrically distant points that are present in a reconstruction stencil on a stretched mesh.



DOI: 10.1002/cnm

Geometrically distant points are often associated with a large observation error in data $U(x, y)$, so that many authors recommend inverse distance weighting of stencil points in order to suppress distant points in a reconstruction stencil and to obtain an accurate reconstructed solution [2–5].

A weighted LS reconstruction is defined by the following merit function $F_w^2$,

$$F_w^2 = \min_{\mathbf{u}} \sum_{i=1}^{N} w(r_{0i})[U(P_i) - u(P_i)]^2$$

where the weight function $w(r_{0i})$ depends on the Euclidian distance $r_{0i}$ between points $P_0$ and $P_i$, $i = 1, 2 \ldots, N$. The solution $\mathbf{u}$ to the normal equations is now obtained as

$$\mathbf{u} = \mathbf{A}_{\text{wls}}^{-1} \mathbf{b}_{\text{wls}}$$

where the matrix $\mathbf{A}_{\text{wls}} = \mathbf{A}^{\text{T}}\mathbf{W}\mathbf{A}$, the vector $\mathbf{b}_{\text{wls}} = \mathbf{A}^{\text{T}}\mathbf{W}\mathbf{U}$, and a diagonal weight matrix $\mathbf{W}$ is defined as

$$W_{ij} = \begin{cases} w(r_{0i}), & i = j, \\ 0 & \text{otherwise} \end{cases} \qquad i, j = 1, 2, \ldots, N$$

The weight function

$$w(r_{0i}) = r_{0i}^{-p}, \quad p = 0, 1, 2, \ldots \tag{10}$$

where $p$ is an integer polynomial degree, is a frequent choice in computational aerodynamics problems [2, 4, 5, 9]. The polynomial degree $p = 0$ is related to an unweighted reconstruction, while $p > 0$ provides inverse distance weighting used to mitigate the impact of distant points in a reconstruction stencil on the accuracy of LS approximation.

Below we discuss the results of a weighted quadratic LS reconstruction for the NACA0012 test case. The maximum error (6) and maximum logarithmic error (9) of a weighted LS reconstruction in 'far-field' domain $D_f$ is given in Table I for various polynomial degrees $p$. It can be seen from the table that assigning weights to stencil points results in a more accurate reconstruction. In particular, the error for a weighted LS reconstruction with polynomial degree $p = 2$ is about 15% smaller than the error for an unweighted reconstruction ($p = 0$). However, heavy weighting of stencil points with $p = 8$ results in a larger error in comparison with the error obtained for the unweighted reconstruction. That happens because heavy weighting of stencil points effectively eliminates them from the stencil, so that the LS approximation misses the data required to quadratically reconstruct function $U(x, y)$.

The results of a weighted LS reconstruction in 'boundary layer' region $D_b$ are shown in Table II. The weight function (10) is not efficient in the domain $D_b$, as the weighting of

Table I. The reconstruction error for quadratic LS approximation in a far field. The maximum error (6) and the maximum logarithmic error (9) are shown for various degrees $p$ of polynomial weight function (10).

| $p$ | 0 | 1 | 2 | 4 | 8 |
|---|---|---|---|---|---|
| $e_{\max_f}$ | $1.27282 \times 10^{-3}$ | $1.09508 \times 10^{-3}$ | $1.08304 \times 10^{-3}$ | $1.14044 \times 10^{-3}$ | $1.38461 \times 10^{-3}$ |
| $e^l_{\max_f}$ | $5.65614 \times 10^{-4}$ | $4.86696 \times 10^{-4}$ | $4.80916 \times 10^{-4}$ | $5.06832 \times 10^{-4}$ | $6.15279 \times 10^{-4}$ |



DOI: 10.1002/cnm

Table II. The reconstruction error for quadratic LS approximation near the airfoil. The maximum error (5) and the maximum logarithmic error (8) is shown for various degrees $p$ of polynomial weight function (10).

| $p$ | 0 | 1 | 2 | 4 | 8 |
|---|---|---|---|---|---|
| $e_{\max_b}$ | 1.38595 | 1.52966 | 1.72857 | 2.18609 | 198.303 |
| $e^l_{\max_b}$ | 2.49593 | 3.23984 | 2.80793 | 2.57411 | 2.79986 |

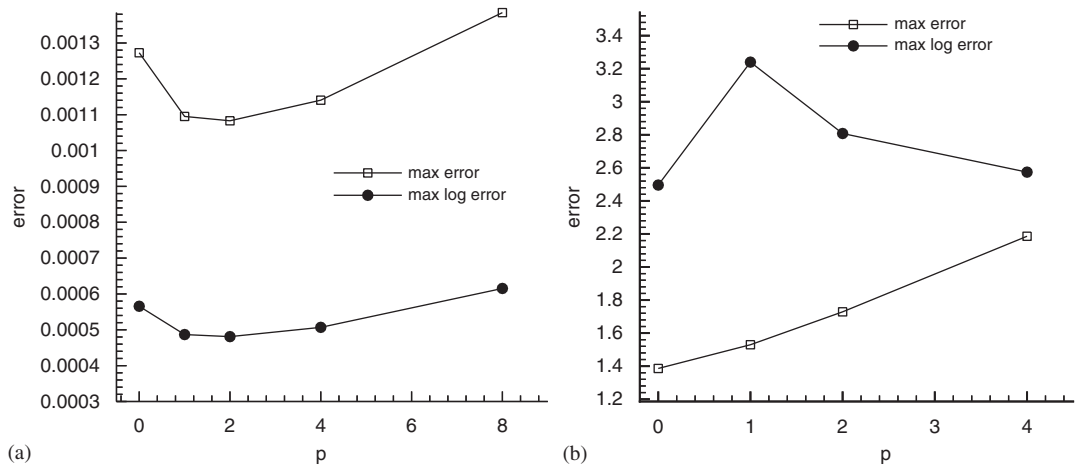


Figure 5. The maximum error and the maximum logarithmic error is shown as a function of degree $p$ of polynomial weight function (10): (a) the error (6) and (9) in a far field and (b) the error (5) and (8) in a near field.

stencil points further increases the maximum error of the reconstruction. One example is given by weighting with $p=8$, where the maximum error becomes $e_{\max_b}=198.303$ after the implementation of weight function (10) in the problem. However, the weight function (10) does not work for the other values of $p$ as well. In particular, weighting with $p=2$, which appears to be optimal in the far field, does not provide an acceptable reconstruction error near the wall.

Figure 5 illustrates the data presented in Tables I and II. The error in a far field is shown in Figure 5(a), while the error near the airfoil is displayed in (b). It can be seen from Figure 5(b) that the maximum logarithmic error slightly decreases when we increase the degree $p$ of the weight function (10), but its value still remains very large. Moreover, the logarithmic error $e^l_{\max}$ is larger than the error $e_{\max}$ in the near field for any polynomial degree $p$ (except the degenerate case $p=8$, which is not shown in the figure for the sake of scaling). This result clearly demonstrates that a weighted LS reconstruction fails to reconstruct a solution function near the wall and another approach is required for an accurate local solution reconstruction.



DOI: 10.1002/cnm

## 3. ELIMINATION OF DISTANT POINTS ON A STRETCHED MESH

It has been shown in the previous section that, while a weighting procedure mitigates the impact of geometrically distant points on an LS reconstruction in a far field, elimination of geometrically distant points from the stencil does not lead to an accurate LS reconstruction on an anisotropic grid generated near the airfoil. In recent work [6] a concept of distant points has been generalized to explain the poor accuracy of a weighted LS method. It has been suggested in [6] that, along with geometrically distant points, numerically distant points may also appear in a reconstruction stencil. A numerically distant point $P_n$ is a stencil point that can be located close to the origin $P_0$, where the function $U(x, y)$ is reconstructed, but the value $U(P_n)$ at such a point still has a large data error that affects the accuracy of an LS reconstruction.

While a detailed discussion of numerically distant points has been provided in [6], below we consider a simple example illustrating the concept. Consider a quadratic function

$$U(x, y) = ax^2 + y \tag{11}$$

where parameter $a = -0.001$. We are interested in LS approximation of the gradient $\partial U/\partial x = 2ax$, $\partial U/\partial y = 1$ at the origin $P_0 = (0, 0)$, where for the sake of simplicity we consider linear reconstruction at point $P_0$

$$u_{\mathrm{LS}}(x, y) - u(P_0) = u_1 x + u_2 y \tag{12}$$

If the function (11) is known at point $P_0$, we have two expansion coefficients $u_1$ and $u_2$ to be defined from LS approximation (12).

Let points $P_i$, $i = 1, \ldots, 4$, be defined as $P_1 = (-H, h_1)$, $P_2 = (0, h_0)$, $P_3 = (H, h_1)$ and $P_4 = (0, -\alpha)$, where $h_0$, $h_1$ and $H$ are fixed positive values with $H \gg 1$, $H \gg h_1$, $h_1 \gg h_0$ (see Figure 6). The reconstruction stencil $\{P_1, P_2, P_3, P_4\}$ results in the following design matrix:

$$\mathbf{A} = \begin{bmatrix} -H & h_1 \\ 0 & h_0 \\ H & h_1 \\ 0 & -\alpha \end{bmatrix}$$

The data vector is $\mathbf{U} = (aH^2 + h_1, h_0, aH^2 + h_1, -\alpha)^{\mathrm{T}}$. The LS method (3) approximates the gradient $(u_1, u_2)$ at point $P_0$ as

$$u_1 = 0, \quad u_2 = \frac{2h_1(aH^2 + h_1) + h_0^2 + \alpha^2}{\alpha^2 + h_0^2 + 2h_1^2} = 1 + \frac{2ah_1H^2}{\alpha^2 + h_0^2 + 2h_1^2} \tag{13}$$

while the exact gradient is $\nabla U(P_0) = (0, 1)$.

The gradient component $u_2$ depends on the parameter $\alpha$. Let the accuracy $\varepsilon$ of the gradient approximation be defined as

$$|u_2 - \partial U(P_0)/\partial y| = \varepsilon \tag{14}$$

Substituting the approximate and the exact gradient into (14) we obtain

$$\frac{2|a|h_1H^2}{\alpha^2 + h_0^2 + 2h_1^2} = \varepsilon, \quad \alpha^2 = \frac{2|a|h_1H^2}{\varepsilon} - h_0^2 - 2h_1^2$$



DOI: 10.1002/cnm

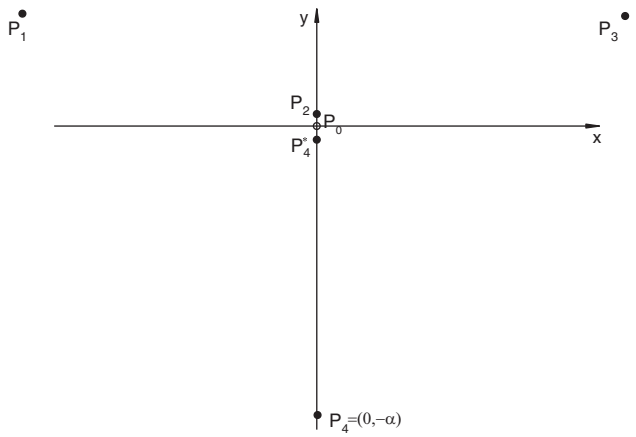


Figure 6. Example of numerically distant points in a reconstruction stencil. The stencil $\{P_1, P_2, P_3, P_4\}$ provides the reconstruction with prescribed accuracy $\varepsilon$, while the stencil $\{P_1, P_2, P_3, P_4^*\}$ contains a numerically distant point $P_4^*$ that affects the accuracy of the reconstruction.

For the accuracy $\varepsilon \sim |a| = 10^{-3}$, the estimate of $\alpha$ becomes

$$\alpha \sim \sqrt{h_1} H \tag{15}$$

where the condition $H \gg h_1$ is taken into account. Consider $H = 20,\ h_1 = 0.5,\ h_0 = 0.01$. Taking $\alpha = 15$ in the reconstruction (13) we obtain $u_2 = 0.9982$. Meanwhile, if we take $\alpha = \alpha^* = 0.01$, the condition (15) is broken and we have $u_2 = 0.2003$. Thus, a reconstruction stencil $\{P_1, P_2, P_3, P_4^*\}$ shown in Figure 6 contains a numerically distant point $P_4^* = (0, -\alpha^*)$. Taking the data $U(x, y)$ at point $P_4^*$ results in a large reconstruction error, despite point $P_4^*$ being located close to the origin.

Let us notice that a conclusion about the numerically distant points in a reconstruction stencil depends essentially on a function $U(x, y)$ under consideration. Since an analytic solution $U(x, y)$ is not available in practical computations, it is difficult to recognize numerically distant points that are captured by a reconstruction stencil on an irregular mesh. Moreover, examples designed in [6] demonstrated that weighting of stencil points does not guarantee that numerically distant points will be eliminated from a reconstruction stencil, as their data error does not depend on the distance to the origin. Thus, it has been suggested in [6] that in some cases it may be helpful to minimize the number of stencil points in order to eliminate *a priori* numerically distant points from the stencil. The idea is to reconstruct a function over a compact stencil $S_C$ which is defined as a set of four grid nodes belonging to the two grid cells that share a given edge (see stencil III in Figure 2). Below we discuss an example of a solution function, where a reconstruction on a compact stencil eliminates numerically distant points and results in more accurate solution approximation.

### *3.1. Anisotropic basis functions for an LS reconstruction*

A main difficulty arising in consideration of a compact stencil $S_C$ is that it does not provide data for a quadratic reconstruction. The stencil $S_C$ consists of four grid points, while at least six grid points are required to determine the coefficients of a quadratic polynomial. Hence we need to use additional information about a solution function in order to define all fitting parameters for a



DOI: 10.1002/cnm

quadratic reconstruction. Obviously the information about the solution, that allows one to recover the data missed when we reduce the number of stencil points, is not always available in the problem. However, in some important cases it becomes possible to enhance the function resolution on a compact stencil. Below we present one such example where the idea of anisotropic basis functions originally developed in [20] is employed in order to provide accurate reconstruction on a compact stencil. While the approach discussed below cannot be applied to any reconstruction problem, this example, nevertheless, clearly demonstrates that solution information is very important if we want to get accurate quadratic LS reconstruction near the wall. This subsection provides a brief outline of anisotropic basis functions for a quadratic reconstruction.

For the sake of further discussion, let us introduce the following definition of an 'anisotropic' solution.

*The function* $u(x, y)$ *is called* '*anisotropic*' *at point* $(x_0, y_0)$, *if the following condition holds*:

$$\frac{\partial^2 u}{\partial \eta^2} = 0 \tag{16}$$

*where the direction* $\boldsymbol{\eta}$ *is orthogonal to the gradient vector, that is* $(\nabla u, \boldsymbol{\eta}) = 0$.

The concept of anisotropic basis functions is based on a simple observation that, if a function has a strong gradient, we can enhance its approximation by using a greater number of basis functions related to the gradient direction in the expansion (1). This idea is somewhat similar to $p$-refinement in discretization schemes, except the total number of basis functions used for the approximation is not increased. Consider the rotation mapping of the $(x, y)$-plane onto the $(\xi, \eta)$-plane

$$\begin{aligned} \xi &= x\cos\delta + y\sin\delta \\ \eta &= -x\sin\delta + y\cos\delta \end{aligned} \tag{17}$$

where $\delta$ is the angle between the $x$-axis and the $\xi$-axis. Since the transformation (17) is linear, basis functions $\phi_m$, $m = 0, 1, \ldots, M$, in the expansion (1) can be replaced by another set $\tilde{\phi}_m$, $m = 0, 1, \ldots, M$, where the new basis functions are

$$\tilde{\phi}_m(\xi, \eta) = (\xi - \xi_0)^\alpha (\eta - \eta_0)^\beta, \quad \alpha + \beta = 0, 1, \ldots, M$$

and the coordinates $\xi_0$ and $\eta_0$ are given by the transformation (17) of the coordinates $x_0$ and $y_0$, respectively. The quadratic approximation (2) in the new basis is

$$u(\xi, \eta) = u_0 + u_1(\xi - \xi_0) + u_2(\eta - \eta_0) + u_3(\xi - \xi_0)^2 + u_4(\xi - \xi_0)(\eta - \eta_0) + u_5(\eta - \eta_0)^2 \tag{18}$$

The expansion coefficients $u_k$ are now determined by derivatives $\partial^k u(\xi, \eta)/\partial\xi^\alpha \partial\eta^\beta$, $\alpha + \beta = k$, in the $(\xi, \eta)$-coordinates.

Let now $\xi$ be the gradient direction, so that the angle $\delta$ between the $\xi$-axis and the $x$-axis is defined as

$$\cos\delta = \frac{(\nabla u)_1}{\|\nabla u\|}, \quad \sin\delta = \frac{(\nabla u)_2}{\|\nabla u\|}$$

where $(\nabla u)_i$, $i = 1, 2$, are components of the gradient vector and $\|\nabla u\| = \sqrt{(\nabla u)_1^2 + (\nabla u)_2^2}$. The definition (16) allows one to use a new set of basis functions

$$\{\tilde{\phi}(\xi, \eta)\} = (1, (\xi - \xi_0), (\xi - \xi_0)^2, (\xi - \xi_0)(\eta - \eta_0)) \tag{19}$$



DOI: 10.1002/cnm

for a quadratic LS reconstruction at point $(x_0, y_0)$, as we have

$$u_2 = \frac{\partial u}{\partial \eta} = 0$$

for the gradient direction and

$$u_5 = \frac{1}{2}\frac{\partial^2 u}{\partial \eta^2} = 0$$

for an anisotropic function. Hence, a compact stencil becomes adequate to the reconstruction task, as only four fitting parameters are now required for a quadratic reconstruction.

### *3.2. Reconstruction on a compact stencil*

In this subsection, we implement anisotropic basis function in an LS reconstruction problem to obtain a more accurate LS reconstruction on a given grid. An anisotropic reconstruction (19) can be illustrated by a simple example where a single reconstruction stencil is considered in a boundary layer region. We consider a fragment of a computational grid shown in Figure 3(a), where a solution function $U(x, y)$ is anisotropic near the wall. The gradient direction is a direction normal to the wall (vector **n** in Figure 7).

Our goal is to reconstruct the function $U(x, y)$ at point $P_0$ and to compare the result with the available solution $U(P_0) = 2.109 \times 10^{-3}$. The procedure to compute the 'exact' solution $U(P_0)$ has been discussed in Section 2. A reconstruction stencil $S_l$ used for a quadratic reconstruction consists of eight points (see Figure 3(a)). A quadratic LS reconstruction (2) weighted with $p = 2$ gives the solution value $u_{\mathrm{LS}}(P_0) = 3.356 \times 10^{-4}$ on stencil $S_l$, so that the reconstruction error (4) at point $P_0$ is $e(P_0) = 1.7734 \times 10^{-3}$. The inaccurate reconstruction at point $P_0$ results in a non-monotone solution near the wall as shown in Figure 7(a).

Let us apply the anisotropic basis functions in the problem. A compact stencil $S_{\mathrm{C}}$ is formed of points $P_1$ through $P_4$. In practical computations the gradient direction can be evaluated from a linear

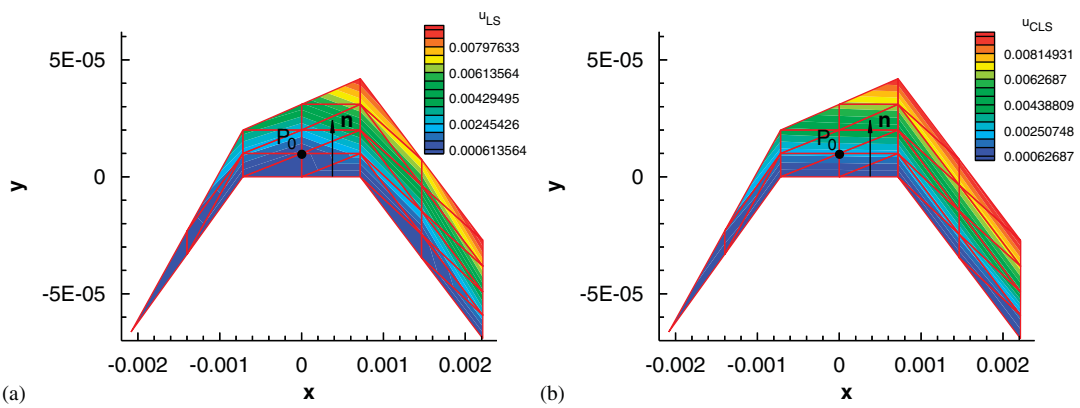


Figure 7. The example of a quadratic LS reconstruction near the wall: (a) an LS reconstruction over a standard stencil $S_l$ shown in Figure 3(a) results in an inaccurate solution at point $P_0$ and (b) a compact stencil $S_{\mathrm{C}} = \{P_1, P_2, P_3, P_4\}$ (see Figure 3) provides an accurate quadratic reconstruction at point $P_0$.



DOI: 10.1002/cnm

reconstruction considered over a compact stencil. We first use the stencil $S_C$ to compute the linear function (12) and consider the expansion coefficients in (12) as $u_1 \approx \partial u/\partial x$ and $u_2 \approx \partial u/\partial y$. The gradient direction is then evaluated as $\cos\delta \approx u_1/\|\nabla u\|$, $\sin\delta \approx u_2/\|\nabla u\|$, and we can apply the transformation (17) along with basis functions (19) for a quadratic LS reconstruction at point $P_0$. The quadratic LS reconstruction on a compact stencil $S_C$ provides a much better result, $u_{\mathrm{CLS}}(P_0) = 2.123 \times 10^{-3}$, and the error (4) now is $e(P_0) = 1.41 \times 10^{-5}$. Thus, the information about the gradient direction allows one to obtain an accurate and monotone solution near the wall (see Figure 7(b)).

We now consider the NACA0012 test case discussed in Section 2 to re-compute an LS reconstruction on a compact stencil. Let us emphasize it again that our purpose is to demonstrate the improvement in the accuracy of LS approximation on a given grid only. A more accurate reconstruction obtained on a compact stencil should confirm our hypothesis about numerically distant points that are present on an anisotropic mesh generated near the wall. At the same time, while our approach offers an alternative to a conventional quadratic LS reconstruction, it cannot be generally employed in practical computations, as it requires condition (16) to reduce the reconstruction support to a compact stencil.

Since we cannot evaluate condition (16) beforehand in order to conclude whether the solution is anisotropic in a given grid cell, we elaborate a 'black box' procedure to obtain the best possible result of an LS reconstruction on a given mesh. Namely, we compute the reconstruction error (4) at a given edge midpoint for both quadratic and linear reconstruction on a compact stencil as well as the error for a conventional quadratic reconstruction (2). We then leave a reconstruction that provides the smallest error (4).

A switch between a quadratic and linear reconstruction is implemented in the problem because there are grid cells where numerically distant points appear in a reconstruction stencil, but the solution function is not anisotropic in those cells. A quadratic reconstruction on a compact stencil will give inaccurate results in grid cells where the condition (16) does not hold, so that a linear reconstruction is required if we want to eliminate numerically distant points. On the other hand, a standard quadratic LS method (2) performs well in grid cells, where the solution is not anisotropic and a reconstruction stencil does not contain numerically distant points. Hence, we need to compute the error for a conventional LS reconstruction as well, as we expect that a quadratic reconstruction on standard stencil $S_l$ will provide a smaller error in the latter case.

The results of our numerical experiment are shown in Table III. In the table we present the error of a standard quadratic reconstruction (LS) weighted with $p = 2$ over the grid $G$. The error is compared with that for a 'hybrid' reconstruction on a compact stencil (CLS) computed on grid $G$. Namely, the maximum error $e_{\max_b}$ and the maximum logarithmic error $e^l_{\max_b}$ is obtained for

Table III. The reconstruction error for standard least-squares approximation weighted with $p = 2$ (LS) and least-squares approximation on a compact stencil (CLS).

| | $e_{\max_b}$ | $e^l_{\max_b}$ | $e_{\max_f}$ | $e^l_{\max_f}$ |
|---|---|---|---|---|
| LS | 1.72857 | 2.80793 | $1.08304 \times 10^{-3}$ | $4.80916 \times 10^{-4}$ |
| CLS | 0.371705 | 1.03009 | $9.57454 \times 10^{-4}$ | $4.24763 \times 10^{-4}$ |

The maximum error $e_{\max}$ and the maximum logarithmic error $e^l_{\max}$ is computed in domain $D_b$ near the airfoil and in far-field $D_f$.



DOI: 10.1002/cnm

both approaches in the domain $D_b$ near the airfoil. We also compute the maximum error $e_{\max_f}$ and the maximum logarithmic error $e^l_{\max_f}$ in the far-field domain $D_f$. It can be seen from the table that, while the results of an LS reconstruction on a compact stencil in domain $D_f$ are similar to a weighted quadratic reconstruction (2), a reconstruction on a compact stencil reduces both the maximum error and the maximum logarithmic error in boundary layer region $D_b$. That confirms our assumption about numerically distant points in a boundary layer. Minimizing the number of stencil points and aligning basis functions to the gradient direction allows one to improve the performance of an LS method near the wall.

Meanwhile, although the maximum logarithmic error $e^l_{\max_b}$ significantly decreases, it still remains relatively large in domain $D_b$. This result indicates the presence of grid cells where we miss solution information required for an accurate reconstruction when we minimize the number of stencil points. Hence the issue of numerically distant points requires further study to elaborate a reliable approach for an accurate LS reconstruction on stretched meshes.

It is worth mentioning here a problem of accuracy validation that arises in consideration of an LS reconstruction on irregular meshes. Obviously, a resulting LS reconstruction on a compact stencil is not entirely quadratic in our test case, as the algorithm we use implies that in some grid cells the reconstruction is reduced to a linear polynomial. However, it is not possible to conclude about the order of LS approximation by looking at a reconstruction error obtained on a single grid, and more thorough investigation of a quadratic reconstruction should involve convergence tests that usually require uniform refinement of a computational grid. Meanwhile, the uniform refinement cannot be straightforwardly applied in the problem to obtain a sequence of nested meshes in a boundary layer region, as a solution needs an anisotropic grid near the wall [9]. Thus, another validation procedure should be designed in order to verify the accuracy of an LS method on stretched meshes. This task is considered as a topic of future work.

To conclude this section, we demonstrate an example of an LS reconstruction on a compact stencil for the NACA0012 test case. The reconstruction results are presented over a grid fragment near the wall as shown in Figure 4. While a conventional quadratic LS reconstruction results in a non-monotone solution $u_{\mathrm{LS}}(x, y)$ shown in Figure 8(a), the use of a compact stencil allows one to get rid of solution oscillations. It can be seen from Figure 8(b) that a reconstructed solution $u_{\mathrm{CLS}}(x, y)$ is a monotone function in the direction normal to the wall.

## 4. CONCLUDING REMARKS

In our paper we have discussed a local LS reconstruction on anisotropic unstructured grids. It has been shown that using a higher-order (quadratic) polynomial in an LS reconstruction procedure does not maintain the accuracy of the reconstruction when irregular geometries are considered. Moreover, weighting of stencil points does not improve the accuracy of the method. This result contradicts a widespread viewpoint that a weighting procedure results in a more accurate reconstruction, as weighting eliminates distant points that are usually associated with a large error in data used for the reconstruction. The above contradiction can be resolved by admitting that, while a weighting procedure deals with geometrically distant points, another type of distant points may appear in a reconstruction stencil on anisotropic meshes. Those points, called numerically distant points in the paper, are not geometrically remote, but they still have a large data error that affects the accuracy of LS approximation.



DOI: 10.1002/cnm

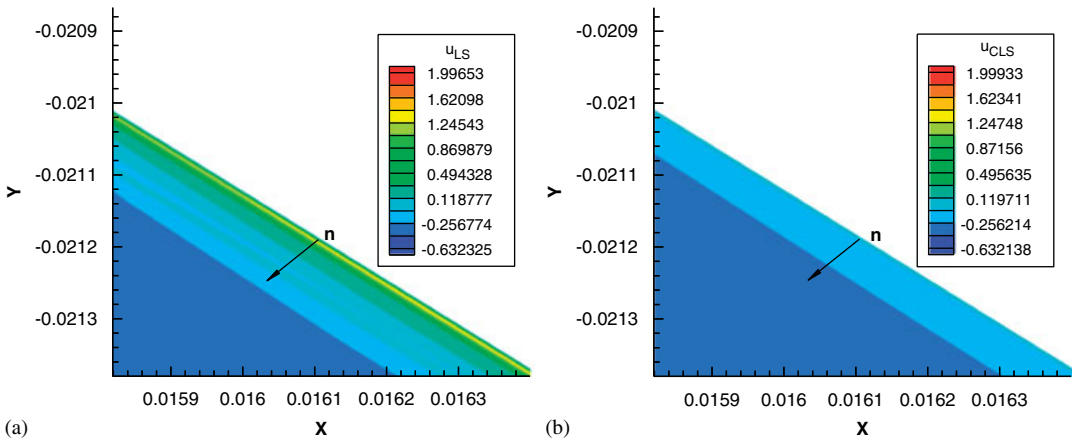


Figure 8. Results of an LS reconstruction on a stretched mesh near the wall: (a) a standard quadratic reconstruction shown also in Figure 4(b) is a non-monotone function in the direction **n** normal to the wall and (b) an LS reconstruction on a compact stencil results in a monotone solution on the same grid.

The concept of numerically distant points has been illustrated in the paper by consideration of a compact stencil that minimizes the total number of stencil points. We have compared a weighted LS reconstruction that only eliminates geometrically distant points with a reconstruction on the compact stencil. The purpose of this numerical experiment is to demonstrate that numerically distant points still remain in a reconstruction stencil after the implementation of a weighting procedure. An approach developed in the paper has shown the advantages of a compact stencil in grid subdomains where a solution function has a strong gradient that requires the generation of a stretched mesh. While the considered approach is restrained by condition (16) that prevents using a compact stencil for an arbitrary function, the test case discussed in the paper clearly indicates the problem of optimal stencil selection that arises in practical computations. In other words, our computations show that solution information rather than grid geometry is crucial for an LS method on irregular meshes. A reliable algorithm of detection of numerically distant points in a reconstruction stencil should help one to get a more accurate LS reconstruction.

Finally, let us notice here that the accuracy of an LS reconstruction on irregular meshes is a challenging task where, in our opinion, investigation of model test cases cannot replace dealing with real-life computations (cf. [11]). Our numerical experience with the problem shows that stencil points with a large data error appear on grids that are not properly refined to accommodate solution features. Hence we may expect numerically distant points in practical computations where a solution is not resolved on coarse meshes. On the other hand, consideration of a test problem, where an analytical solution is available, usually allows one to generate a mesh that is well adapted to a solution function. Reconstruction stencils defined on such a mesh will unlikely contain numerically distant points. Indeed, numerous test cases, where a computational mesh was carefully generated, demonstrated good accuracy of a weighted LS method [3, 5, 15]. Thus, the design of adequate test cases to verify the results of an LS reconstruction on irregular meshes is an important problem, which is considered as a topic of future work.



DOI: 10.1002/cnm

ACKNOWLEDGEMENTS

This research was supported by The Boeing Company under contract 66-ZB-B001-10A-533. The author wishes to thank Dr Forrester Johnson of Boeing who provided test cases for this work.

REFERENCES

1. Aftosmis MJ, Gaitonde D, Tavares TS. Behaviour of linear reconstruction techniques on unstructured meshes. *AIAA Journal* 1995; **33**(1):2038–2049.
2. Barth TJ. A three-dimensional upwind Euler solver for unstructured meshes. *AIAA 91-1548*, 1991.
3. Haselbacher A. On constrained reconstruction operators. *AIAA 2006-1274*, 2006.
4. Mavriplis DJ. Revisiting the least-square procedure for gradient reconstruction on unstructured meshes. *AIAA 2003-3986*, 2003.
5. Ollivier-Gooch C, Van Altena M. A high-order-accurate unstructured mesh finite-volume scheme for the advection–diffusion equation. *Journal of Computational Physics* 2002; **181**:729–752.
6. Petrovskaya NB. Discontinuous weighted least-squares approximation on irregular grids. *Computer Modeling in Engineering and Sciences* 2008; **32**(2):69–84.
7. Anderson WK. A grid generation and flow solution method for the Euler equations on unstructured grids. *Journal of Computational Physics* 1994; **110**(1):23–38.
8. Barth TJ, Jespersen DC. The design and application of upwind schemes on unstructured meshes. *AIAA 89-0366*, 1989.
9. Venkatakrishnan V, Allmaras SR, Johnson FT, Kamenetskii DS. Higher order schemes for the compressible Navier–Stokes equations. *AIAA 2003-3987*, 2003.
10. Anderson WK, Bonhaus DL. An implicit upwind algorithm for computing turbulent flows on unstructured grids. *Computers and Fluids* 1994; **23**:1–21.
11. Thomas JL, Diskin B. Towards verification of unstructured-grid solvers. *AIAA-2008-666*, 2008.
12. Kenney JF, Keeping ES. Linear regression and correlation. *Mathematics of Statistics*, *Part 1* (3rd edn). Van Nostrand: Princeton, NJ, 1962; 252–285.
13. Sonar T. Difference operators from interpolating moving least squares and their deviation from optimality. *Mathematical Modelling and Numerical Analysis* 2005; **39**(5):883–908.
14. Smith TM *et al.* Comparison of reconstruction techniques for unstructured mesh vertex centered finite volume schemes. *AIAA 2007-3958*, 2007.
15. Haselbacher A, Vasilyev OV. Commutative discrete filtering on unstructured grids based on least-squares techniques. *Journal of Computational Physics* 2003; **187**(1):197–211.
16. Alexa M *et al.* Computing and rendering point set surfaces. *IEEE Transactions on Visualization and Computer Graphics* 2003; **9**(1):3–5.
17. Atluri SN, Shen S. The basis of meshless domain discretization: the meshless local Petrov–Galerkin (MLPG) method. *Advances in Computational Mathematics* 2005; **23**:73–93.
18. Martynov AA, Medvedev SYu. A robust method of anisotropic grid generation. *Grid Generation*: *Theory and Applications*. Computing Centre RAS: Moscow, 2002; 266–275.
19. Hughes TJR, Brooks A. A multidimensional upwind scheme with no crosswind diffusion. *Finite Element Methods for Convection Dominated Flows*. ASME: New York, 1979.
20. Petrovskaya NB, Wolkov AV, Lyapunov SV. Modification of basis functions in high order discontinuous Galerkin schemes for advection equation. *Applied Mathematical Modelling* 2008; **32**(5):826–835.



DOI: 10.1002/cnm